Relating ^{139}La Quadrupolar Coupling Constants to Polyhedral Distortion in Crystalline Structures

*Alexander L. Paterson, Margaret A. Hanson, Ulrike Werner-Zwanziger, Josef W. Zwanziger**

Department of Chemistry, Dalhousie University, PO Box 15000, Halifax, NS B3H 4R2, Canada

*Corresponding author.

Tel: +1 (902) 494-1960. Fax: +1 (902) 494-1310. E-mail: jzwanzig@dal.ca

Abstract

A broad series of crystalline lanthanum oxide-based materials has been investigated through high-field ^{139}La solid state nuclear magnetic resonance (ssNMR) spectroscopy and ab initio density functional theory (DFT) calculations. The ^{139}La NMR spectra of $LaBGeO_5$, $LaBSiO_5$, $LaBO_3$, $LaPO_4 \cdot 1.8H_2O$, $La_2(SO_4)_3 \cdot 9H_2O$**,** and $La_2(CO_3)_3 \cdot 8H_2O$ are reported for the first time. Both newly reported and literature values of ^{139}La quadrupolar coupling constants (C_Q) are related to various quantitative expressions of polyhedral distortion, including sphericity (Σ) and ellipsoid span (ϵ). The compounds were separated into two groups based upon their polyhedral distortion behaviour: compounds with the general formula $LaMO_3$, where M is a trivalent cation; and compounds with different general formulae. The ^{139}La C_Q of the $LaMO_3$ family was found to correlate best with ϵ. The ^{139}La C_Q of non-$LaMO_3$ compounds correlates adequately to ϵ, but is better described by Σ. The ^{139}La isotropic chemical shift (δ_{iso}^{CS}) of the non-$LaMO_3$ compounds is negatively correlated with the lanthanum coordination number; there is insufficient data from the $LaMO_3$ compounds to draw conclusions relating to chemical shift. DFT calculations of NMR parameters prove to be a sensitive probe of the quality of input geometry, with predicted parameters agreeing with experiment except in cases where the crystal structure is suspect.

Introduction

Lanthanum compounds have a wide variety of applications, including nickel-metal hydride batteries,[1] transparent ferroelectric nanocomposites,[2] medical glassmaking,[3] and both medical and environmental phosphate sequestration[4,5]. Many of these applications involve amorphous materials, complicating the characterization of the lanthanum environment. Solid state nuclear magnetic resonance (ssNMR) is an effective probe of local coordination in non-periodic solids, but has not yet been applied to ^{139}La in amorphous lanthanum compounds. In order to increase the utility of ^{139}La ssNMR as a structural characterization tool, we investigate the relationship between observable ^{139}La ssNMR properties and the distortion of the lanthanum sites in lanthanum oxide-based materials.

The primary NMR-active nucleus of lanthanum, ^{139}La, has several attractive nuclear properties including a complete natural abundance (100%), a nuclear spin of I = 7/2, and a moderate gyromagnetic ratio ($\gamma = 3.801 \cdot 10^7$ rad T^{-1} s^{-1}), all of which contribute to a high receptivity ($1.61 \cdot 10^2$ as compared to ^{29}Si). A moderately high nuclear electric quadrupole moment ($Q = 20$ fm^2)[6] has been the primary barrier to the ssNMR study of ^{139}La. Until the advent of the wideband uniform rate smooth truncation quadrupolar Carr-Purcell Meiboom-Gill (WCPMG) pulse sequence,[7] the breadth of many spectra prevented their timely acquisition, restricting investigations into relatively high symmetry compounds which yield narrow spectra.[8–10] The WCPMG pulse sequence, in conjunction with variable offset cumulative spectra (VOCS) collection, has recently been put to good use in the investigation of a number of both coordination and inorganic lanthanides,[11–13] including $LaScO_3$ [14] and $LaPO_4$ [5].

The lineshape of ^{139}La NMR spectra is primarily due to interactions of the nucleus with the electric field gradient (EFG) tensor. Two parameters describe this interaction: the quadrupolar coupling constant C_Q, and the quadrupolar asymmetry parameter η

$$C_Q = \frac{eQV_{zz}}{h} \quad (1)$$

$$\eta = \frac{V_{yy} - V_{xx}}{V_{zz}} \quad (2)$$

where eQ is the electric quadrupole moment of the nucleus, h is the Planck constant, and $|V_{zz}| \geq |V_{yy}| \geq |V_{xx}|$ are the principal components of the EFG tensor. The magnitude of the quadrupolar coupling constant has commonly been used to infer qualitative deviations from spherical symmetry while the asymmetry parameter provides information regarding axial symmetry.[9,15,16] An additional influence on the lineshape of NMR spectra is chemical shift anisotropy (CSA). The CSA tensor is defined similarly to the EFG tensor, with principal components $\delta_{11} \geq \delta_{22} \geq \delta_{33}$. This work uses the Herzfeld-Berger convention[17] for describing the influence of CSA on NMR lineshapes.

Note that the principal directions of the CSA tensor need not coincide with those of the EFG tensor, and neither need coincide with "obvious" crystallographic directions unless satisfying the symmetry requirements of the unit cell. Nevertheless, if correlations between these tensors and crystal structures can be established for a class of materials, then extension to structurally uncharacterized samples is possible. Indeed, many studies have attempted to link the above NMR properties to structural features: for example, Pan et al. used ^{6}Li magic angle spinning (MAS) NMR to probe the presence of Cr^{3+} in the lithium coordination sphere[18]; ^{11}B MAS NMR is routinely used to quantify relative proportions of three- and four-coordinate boron; Willans et al. were able to establish a link between ^{139}La isotropic chemical shift and lanthanum coordination number in organic lanthanum coordination compounds using solid-state NMR[13]; and Michaelis and Kroeker investigated the possibility of relating ^{73}Ge C_Q to octahedral and tetrahedral distortion parameters[15]. While tetrahedral and octahedral distortion parameters are effective in describing differences between real and ideal polyhedra, it is difficult to generalize the method used by Michaelis and Kroeker to polyhedra with higher coordination number. Balić Žunić and Makovicky devised a method involving least-squares fitting of a sphere to the ligands of the coordination polyhedron[19] which provides a novel means of measuring distortion. Various distortion parameters are derived from the relationship between a circumscribed sphere and the ideal polyhedral shape.[20] These parameters have been successfully used to predict the coefficient of thermal expansion in $A_2M_3O_{12}$ materials.[21,22] However, modelling the EFG tensor requires a parameter more sensitive to the specific distortion from spherical symmetry.

Balić Žunić and Makovicky[19] define the sphericity of the coordination polyhedron, which we label Σ, as

$$\Sigma = 1 - \frac{\sigma_{rs}}{r_s} \quad (3)$$

where r_s is the average distance between the centroid of the coordination polyhedron and the ligands, and σ_{rs} is the standard deviation of the same. The centroid of coordination is the point with minimal variation of position with regards to the oxygen ligands, and frequently, but not always, coincides with the position of the La^{3+} cation. The sphericity describes the deviation of the ligand distances from the average distance, which models the general deviation from spherical symmetry.

Beyond considering the isotropic deviation from spherical symmetry, we also consider the anisotropy of the distortion. To this end, we fit the coordination polyhedron with a triaxial ellipsoid (Figure 1). The resulting ellipsoid is defined by its three semi major axes $e_a \leq e_b \leq e_c$. The level of anisotropy of the ellipsoid is described by two parameters derived from the semi major axes: the ellipsoid span, which we will refer to as ϵ, defined by Balić Žunić and Makovicky[23] as

$$\epsilon = \frac{e_c - e_a}{\frac{e_a + e_b + e_c}{3}} \quad (4)$$

and the ellipsoid character (E.C.), which describes how close in length e_b is to the other semi major axes. More precisely, the ellipsoid character is defined in analogy to the optical character.[23] The ellipsoid character is the cosine of the angle between the normals of the two unique circular cross-section of the ellipsoid fitting the polyhedron, as bisected by the longest major axis. Practically, the ellipsoid character ranges from -1, describing an oblate spheroid, to +1, describing a prolate spheroid, while intermediate values indicate that the elipsoid is triaxial. ϵ will range from 0 when the ellipsoid is spherical, and will approach 3 when $e_c \gg e_a$.

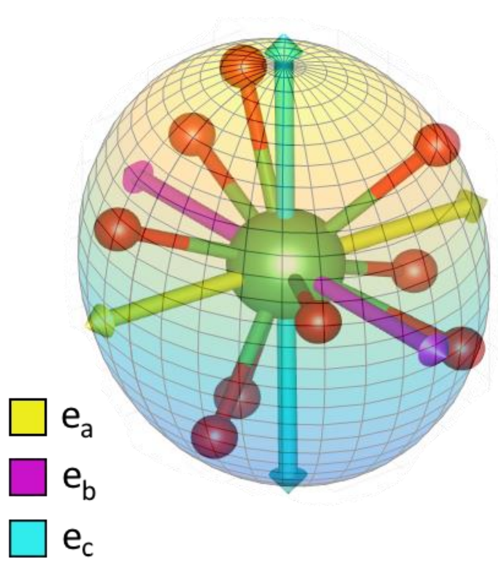

Figure 1: Schematic diagram of triaxial ellipsoid fit to the LaO_9 polyhedron of $LaBGeO_5$.

In this work we use ^{139}La ssNMR in conjunction with density functional theory (DFT) calculations to construct an empirical model relating the distortion of the lanthanum coordination polyhedra to the observed ^{139}La C_Q values. We establish that the ^{139}La C_Q of compounds with the general formula $LaMO_3$ (M = B^{3+}, Al^{3+}, Sc^{3+}, Ti^{3+}, Cr^{3+}, Co^{3+}) is dependent primarily on the ellipsoid span, while the ^{139}La C_Q of other compounds is related to both the ellipsoid span and the sphericity parameter.

Experimental

Synthesis and Characterization

Samples of La_2O_3 (≥ 99.9%), $LaBO_3$ (99.9%), $La_2(CO_3)_3 \cdot xH_2O$ (99.9%), and $La_2(SO_4)_3 \cdot 9H_2O$ (≥ 99.99%) were purchased from Sigma-Aldrich. $LaPO_4 \cdot xH_2O$ (99.99%) was purchased from Alfa Aesar. The above samples were used without further purification. $LaPO_4$ was produced by heating $LaPO_4 \cdot xH_2O$ at 750 °C for 21h in atmosphere. $LaBGeO_5$ glass was produced by grinding stoichiometric amounts of La_2O_3, B_2O_3 (99%, Sigma-Aldrich), and GeO_2 (99.998%, Sigma-Aldrich) in a ceramic mortar and pestle and heating at 1300 °C for 30m in a platinum crucible in atmosphere. The resulting glass was poured into a glass mold pre-heated to 400 °C, and held at 400 °C for 24 h. Crystallization was induced by heating the glass at 950 °C for 12h. The resulting ceramic was ground to powder in an agate mortar and pestle. $LaBSiO_5$ powder was produced by grinding stoichiometric amounts of La_2O_3, B_2O_3, and SiO_2 (Analytical, Sigma-Aldrich) in a ceramic mortar and pestle and heating from 900 °C to 1300 °C over 5 h in a platinum crucible in atmosphere. Identities of both commercial and synthesized samples were confirmed using powder X-ray diffraction. X-ray diffraction experiments were conducted using a Rigaku Ultima IV X-ray diffractometer using a copper anode X-ray tube with a diffracted beam monochromator and a scintillation detector. X-ray diffractograms are available in the supporting information. Thermogravimetric analysis (TGA) was used to characterize the level of hydration of $LaPO_4 \cdot 1.85H_2O$ and $La_2(SO_4)_3 \cdot 9H_2O$ (Figure S8). The level of hydration of $La_2(CO_3)_3 \cdot nH_2O$ was not determined due to contamination of the sample.

NMR Spectroscopy

^{139}La NMR spectra were collected on 9.4T (56.54 MHz ^{139}La frequency) and 16.4 T (98.91 MHz ^{139}La frequency) Bruker Avance NMR spectrometers. Samples were finely ground in an agate mortar and pestle and packed into either 4 mm (16.4 T) or 7 mm (9.4 T) outer diameter ZrO_2 rotors. All spectra were collected under static conditions. The WCPMG pulse sequence[7] was used with WURST-80 (16.4 T) or WURST-20 (9.4 T) pulses[24] of 50 μs duration, sweeping across 500 kHz at a rate of 10 MHz/ms to ensure homogenous excitation. The number of echoes collected varied from 60 to 250 according to the T_2 relaxation of the sample. Spectral slices were collected with a transmitter offset of either approximately 100 kHz or 200 kHz, with the exact value set to an integer multiple of the spikelet separation. The number of slices depended on the breath of the spectral peak. The number of scans per slice varied between 16 and 3192, dependent on sensitivity of the sample. Optimized recycle delays of between 0.1 and 5 s were used. Total experimental time was uniformly less than 2 h. ^{139}La chemical shifts were referenced to a 1.0 M aqueous solution of $LaCl_3$. Spectra were fit using DMFit v20110512[25], WSolids v1.19.2[26], and QUEST v1.1.5[27].

DFT Calculations

Density functional theory calculations were carried out using the ABINIT code[28–31] using the projector-augmented wave (PAW) method[32]. The PAW datasets used varied depending on the structure being investigated. When possible, JTH PAW datasets were used without alteration.[33] In systems where there was significant PAW sphere overlap, custom datasets were used to avoid this problem. Details on the datasets used for each structure are available in the supporting information (Table S1). All calculations were performed using the Perdew, Burke, and Ernzerhof (PBE) generalized gradient approximation (GGA) exchange-correlation functional[34].

Calculations were conducted on crystal structures taken from the Inorganic Crystal Structure Database (ICSD).[35] Optimized plane-wave cutoff energies were used, typically between 30 and 45 hartrees, with PAW fine grid cutoff energies generally between 90 and 150 hartrees. K-point grids were optimized for each structure, but typically had a grid spacing of 0.03 $Å^{-1}$. Specific values for each structure are available in the supporting information (Table S2). EFG parameters were calculated on experimental geometries. Calculations were performed using the WestGrid Grex research facility, with Intel Xeon X6560 2.66 GHz cores. Between 4 and 24 cores were used depending on the fineness of the k-point grid.

Distortion Parameters

Distortion parameters were calculated using the IVTON software.[23] Input structures were obtained from the ICSD,[35] and were also used for DFT calculations. Uncertainties in distortion parameters were either determined through propagation of error or estimated from least-squares variance.

Results

^{139}La NMR spectroscopic parameters, computational results, and distortion parameters are reported in Tables 1 through 3. The presentation of the results for $LaBGeO_5$ and $LaScO_3$ are discussed as representative of the non-$LaMO_3$ and $LaMO_3$ compounds, respectively. The full results and discussion for all other compounds are included in the supporting information.

Table 1. Summary of the experimental ^{139}La NMR parameters.

	$\lvert C_Q \rvert$ (MHz)	η	δ_{iso}^{CS} [a] (ppm)	Ω [b] (ppm)	κ [c]	α [d] (°)	β [d] (°)	γ [d] (°)
La_2O_3	58.6(3)	0.00(2)	620 (10)	500(50) [e]	-1.0(2) [e]	150(150) [e]	90(10) [e]	180(10) [e]
$LaPO_4 \cdot 1.8\ H_2O$	33(1)	1.00(5)	400(20)					
$LaPO_4$	46.7(10) [f]	0.75(3) [f]	36(10) [f]					
$LaBO_3$	23.4(4)	0.68(5)	230(10)	350(30)	0.3(1)	15(5)	0(5)	165(10)
$LaBGeO_5$	85.5(5)	0.30(2)	200(25)	400(200)	0.8(3)	75(75)	15(5)	0(10)
$LaBSiO_5$	90.0(5)	0.35(2)	225(50)					
$La_2(SO_4)_3 \cdot 9H_2O$								
La(1)	52.5(5)	0.00(2)	-175(25)					
La(2)	36.5(5)	0.00(3)	-75(25)					
$La(OH)_3$	22.0(0.5) [e]	0.05(2) [e]	260(20) [e]	80(7) [e]	0.0(1) [e]	80(7) [e]	10(10) [e]	0(10) [e]
$LaAlO_3$	6 [g, h]	0 [g, h]	375(5) [g, h]					
$LaCoO_3$	23.8 [g, i]	0 [g, i]	4230 [g, i]					
$LaCrO_3$	48 [g, i]	0.15 [g, i]	442.5 [g, i]					
$LaTiO_3$	53.2 [g, j]	0.6 [g, j]	N.D.					
$LaScO_3$	61.6(5) [k]	0.10(2) [k]	600(50) [k]	500(200) [k]	0.0(3) [k]			
$LaNbO_4$	36(2) [e]	0.44(5) [e]	295(25) [e]	255(10) [e]	0.40(4) [e]	90(5) [e]	50(5) [e]	270(10) [e]

[a] $\delta_{iso}^{CS} = \frac{1}{3}(\delta_{11}+\delta_{22}+\delta_{33})$. [b] $\Omega = \delta_{11}-\delta_{33}$. [c] $\kappa = \frac{3(\delta_{22}-\delta_{iso}^{CS})}{\delta_{11}-\delta_{33}}$. [d] α, β, γ are the Euler angles. [e] Spencer et al.[16] [f] Dithmer et al.[5] [g] These values were provided without uncertainties; discussion of the reliability of these values is found in the Supporting Information. [h] Dupree et al.[9] [i] Bastow[10] [j] Furukawa et al.[36] [k] Johnston et al.[14]

Table 2. Summary of the calculated ^{139}La NMR parameters

	C_Q (MHz)	η
La_2O_3	60.61	0.00
$LaPO_4 \cdot 0H_2O$	-136.18	0.50
$LaPO_4$	53.67	0.56
$LaBO_3$	-28.79	0.57
$LaBGeO_5$	-89.03	0.32
$LaBSiO_5$	-109.95	0.05
$La_2(SO_4)_3 \cdot 9H_2O$		
La(1)	-59.10	0.00
La(2)	-36.46	0.00
$La(OH)_3$	-29.49	0.00
$LaAlO_3$	8.44	0.00
$LaCoO_3$	20.99	0.00
$LaCrO_3$	-47.22	0.32
$LaScO_3$	-65.17	0.08
$LaNbO_4$	39.46	0.50

Table 3. Collected distortion parameters.

	CN	Σ	e_a (Å)	e_b (Å)	e_c (Å)	ϵ	E.C.
La_2O_3	7	0.960(5)	2.481(2)	2.481(2)	2.731(2)	0.098(2)	1.00(1)
$LaPO_4$	9	0.965(2)	2.415(1)	2.574(1)	2.796(1)	0.147(1)	0.05(1)
$LaBO_3$	9	0.963(1)	2.331(1)	2.721(1)	2.741(1)	0.157(1)	-0.92(1)
$LaBGeO_5$	9	0.951(2)	2.359(1)	2.713(1)	2.744(1)	0.148(1)	-0.87(1)
$LaBSiO_5$	10	0.943(4)	2.350(1)	2.713(1)	2.808(1)	0.175(1)	-0.67(1)
$La_2(SO_4)_3 \cdot 9H_2O$							
La(1)	12	0.960(2)	2.463(1)	2.837(1)	2.837(1)	0.138(1)	-1.00(1)
La(2)	9	0.9927(1)	2.514(1)	2.514(1)	2.585(1)	0.028(1)	1.00(1)
$La(OH)_3$	9	0.9927(1)	2.551(1)	2.551(1)	2.620(1)	0.027(1)	1.00(1)
$LaAlO_3$	12	0.963(1)	2.67(1)	2.70(1)	2.70(1)	0.01(1)	-1.00(1)
$LaCoO_3$	12	0.931(5)	2.67(4)	2.78(4)	2.78(4)	0.04(3)	-1.00(1)
$LaCrO_3$	12	0.909(9)	2.58(6)	2.81(6)	3.03(6)	0.16(5)	-0.15(1)
$LaTiO_3$	8	0.956(3)	2.384(1)	2.462(1)	2.872(1)	0.190(1)	0.60(1)
$LaScO_3$	8	0.935(6)	2.334(1)	2.432(1)	3.032(1)	0.269(1)	0.61(1)
$LaNbO_4$	8	0.9877(4)	2.419(1)	2.478(1)	2.606(1)	0.075(1)	0.32(1)

Lanthanum Borogermanate

$LaBGeO_5$ (LBG) is an example of the stillwellite rare earth mineral[37] that has been extensively studied for its ferroelectric properties.[38–40] It is a remarkably efficient glass former, given its high lanthanum content. LBG glass is an effective transparent ferroelectric nanocomposite material, due to the shared stoichiometry between crystalline and glassy phases.[2] LBG has been previously studied using Raman spectroscopy,[41] computational methods,[42] and ^{11}B magic angle spinning NMR spectroscopy,[2] but as of yet has not been investigated using ^{139}La NMR. As a member of the stillwellite family, LBG is of trigonal space group P_{31}, with three formula units per unit cell. The environment of the single lanthanum site in LBG is ninefold coordinate to oxygen, with contributions from both the GeO_4 and BO_4 tetrahedra. La-O bond range from 2.41 Å to 2.74 Å, with an average of 2.60 Å. There are no obvious symmetry elements present within the lanthanum polyhedron.

The ^{139}La ssNMR spectrum of LBG acquired at 16.4 T is presented in Figure 2. The spectrum is extremely broad, spanning approximately 12 000 ppm. It is fit using a C_Q of 85.5 ± 0.5 MHz and η of 0.30 ± 0.02. The spectrum is overwhelmingly quadrupolar in character, with only a minor influence from CSA. Using spectra collected at 9.4 T and 16.4 T we fit the spectra with CSA value of Ω = 400 ± 200 ppm, κ = 0.8 ± 0.3, α = 75 ± 75°, β = 15 ± 5°, and γ = 0 ± 10°. When fitting the spectrum acquired at the lower field strength (9.4 T), the high-field approximation is less valid due to the extreme breadth of the peak; as such, we must fit it exactly, rather than through perturbation theory.[27]

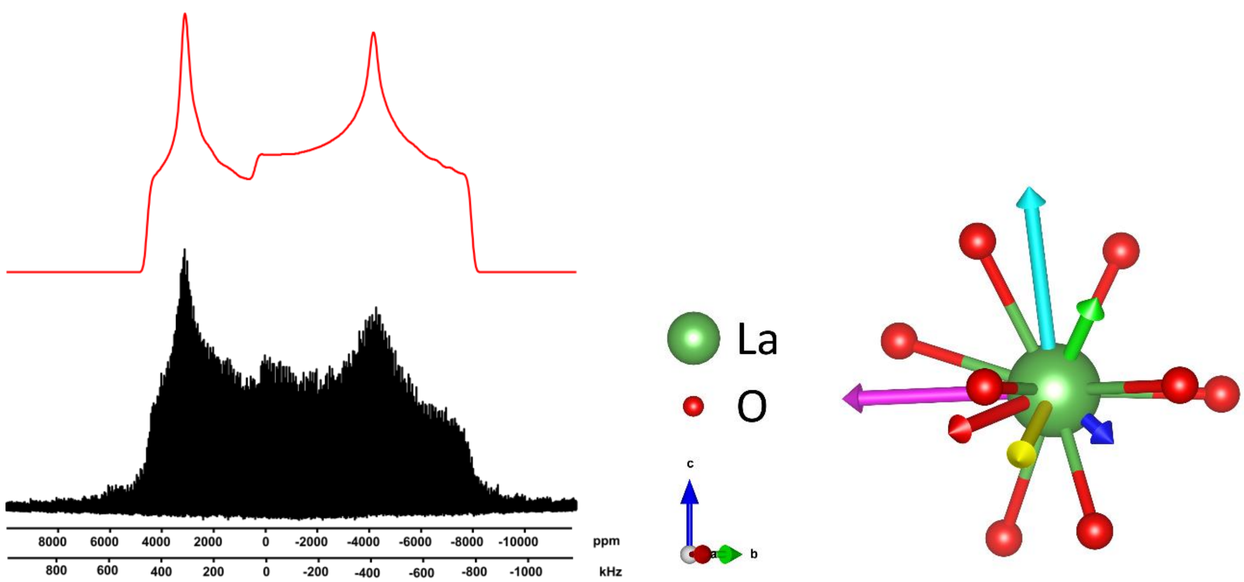

Figure 2. Left: Static ^{139}La NMR spectrum of $LaBGeO_5$ at 16.4 T. Analytical simulation is show in red. The EFG parameters used are reported in Table 1. Right: First coordination sphere of LaO_9 in $LaBGeO_5$. The V_{xx}, V_{yy}, and V_{zz} components are displayed as blue, green, and red, respectively. The e_a, e_b, and e_c semi major axes are in yellow, magenta, and teal respectively.

DFT calculations on the experimental LBG geometry[43] yield a ^{139}La C_Q of -89 MHz and η of 0.32. This is in excellent agreement with the experimental results (C_Q = 85.5 ± 0.5 MHz and η = 0.30 ± 0.02). The V_{zz} component of the EFG tensor is not directed toward any specific structural feature, but is generally aligned with GeO_4 tetrahedra. The La-O bond closest to the V_{zz} vector links a GeO_4 tetrahedron with two LaO_9 polyhedra, but the bond and the vector are not parallel (Figure 2).

The ellipsoid fit to the LaO_9 polyhedron is triaxial, with e_a = 2.359 ± 0.001 Å, e_b = 2.713 ± 0.001 Å, and e_c = 2.744 ± 0.001 Å. The shortest semi major axis, e_a, is in close proximity to the V_{zz} component. The ellipsoid is significantly distorted from spherical symmetry, with ϵ = 0.148 ± 0.001. The ellipsoid is oblate in nature, with a character of -0.87 ± 0.01.

Lanthanum Scandate

$LaScO_3$ is the lanthanum perovskite most recently studied by ^{139}La ssNMR spectroscopy, and the only one published to date that has been studied by WCPMG.[14] $LaScO_3$ is in the Pbnm space group with four formula units per unit cell. The lanthanum environment is eightfold, with La-O bonds ranging from 2.40 Å to 2.88 Å, with an average bond length of 2.62 Å.[14] Like $LaTiO_3$, the LaO_8 polyhedron is best described as a distorted square antiprism.

Johnston et al. fit the ^{139}La WCPMG ssNMR spectrum of $LaScO_3$ with a C_Q of 61.6 ± 0.5 MHz and an η of 0.10 ± 0.02, [14] and carried out DFT calculations on the $LaScO_3$ structure reported by Liferovich and Mitchell[44]. In order to obtain the principal components of the EFG tensor, we conducted our own DFT calculations on the experimental geometry reported by Johnston et al.;[14] our calculations yielded a C_Q of -65.2 MHz and an η of 0.08. The V_{xx} component is parallel to both the crystallographic c axis and the ellipsoid e_c axis, hence the V_{yy} and V_{zz} components are in the plane defined by the a and b crystallographic axes. Our computed value of η is comparable with the computed value reported by Johnston et al. (0.08 vs. 0.13) as well as with their experimental value (0.08 vs. 0.10 ± 0.02), but our computed value of C_Q is significantly different than their computed value (-65.17 MHz vs. -51.66 MHz)[14]. Our computed value of the ^{139}La C_Q is in good agreement with the experimental value reported by Johnston et al. (-65.17 MHz vs 61.6 ± 0.5 MHz).[14] This difference is likely due to the difference in initial starting geometries; where we used the structure reported by Johnston et al.[14], they began from the structure reported by Liferovich and Mitchell[44].

The ellipsoid used to fit the LaO_8 polyhedron is significantly distorted, with e_a = 2.334 ± 0.001 Å, e_b = 2.432 ± 0.001 Å, and e_c = 3.032 ± 0.001 Å (Figure 3). The ellipsoid is generally prolate, with a character of 0.61 ± 0.01, and shows the greatest distortion of all ellipsoids modelled in this study, with a value of 0.269 ± 0.001. The largest semi major axis e_c is aligned with the crystallographic c axis, while the other two semi major axes are slightly angled from La-O1 bonds (as labelled by Johnston et al.[14]). The shortest semi major axis is very nearly parallel with a La-O bond of length 2.532 Å, while the e_b axis is displaced from a La-O bond of length 2.396 Å by the same angle. Similar behaviour is observed in the isostructural $LaTiO_3$.

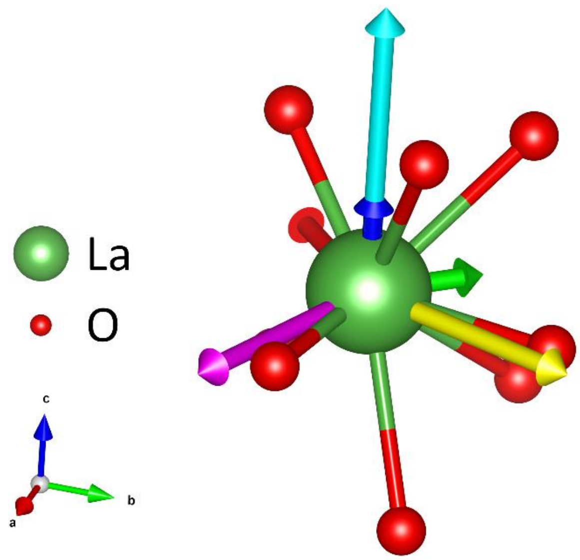

Figure 3. First coordination sphere of LaO_8 in $LaScO_3$. The V_{xx}, V_{yy}, and V_{zz} components are displayed as blue, green, and red, respectively. The e_a, e_b, and e_c semi major axes are in yellow, magenta, and teal respectively.

Discussion

Coordination Number

The relationship between lanthanum coordination number (CN) and ^{139}La NMR properties has previously been investigated by Willans et al.[13] They found no correlation between La coordination number and C_Q or Ω, but they did find a strong relationship between the La coordination number and ^{139}La δ_{iso}^{CS}. When analyzing our data, we were unable to establish a generally strong relationship between the coordination number and δ_{iso}^{CS} ($R^2 = 0.11$). The quality of the fit improves dramatically ($R^2 = 0.63$) when considering compounds of general formula $LaMO_3$ (M = B^{3+}, Co^{3+}, Cr^{3+}, Sc^{3+}, Ti^{3+}) separately from the other lanthanum compounds (Figure 4). The isotropic chemical shift of the non-$LaMO_3$ compounds decreases as coordination number increases, consistent with the observations of Willans et al. It is difficult to conclusively evaluate the trend of δ_{iso}^{CS} in the $LaMO_3$ compounds due to insufficient data, as the δ_{iso}^{CS} of $LaTiO_3$ has not been reported and the δ_{iso}^{CS} of $LaCoO_3$ is anomalously high; this is proposed to be caused by transferred hyperfine interactions.[10] The coordination number alone is clearly insufficient to relate the ^{139}La isotropic chemical shift to local structure, but it is nonetheless useful in assigning NMR peaks in structures with multiple lanthanum sites (e.g. $La_2(SO_4)_3 \cdot 9H_2O$). The range of δ_{iso}^{CS} reported in this study is approximately 900 ppm, while the range of chemical shifts reported in the literature spans approximately 1200 ppm[45] (excluding samples affected by hyperfine interactions, e.g. $LaCoO_3$). ^{139}La ssNMR peaks are often broadened past this chemical shift range, limiting the potential effects of CSA in ultrawide compounds.

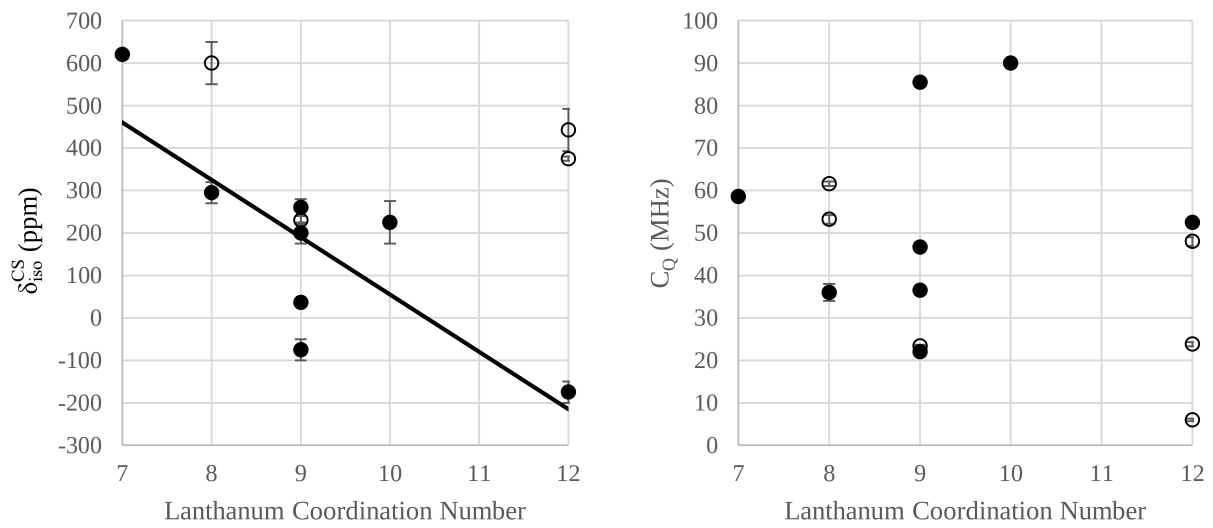

Figure 4. Relationship between the La coordination number and the ^{139}La isotropic chemical shifts (left) and quadrupolar coupling constants (right). Filled circles (●) indicate compounds of the non-$LaMO_3$ family, while open circles (○) indicate $LaMO_3$ compounds. The solid line in the left plot

shows the relationship between La CN and ^{139}La δ_{iso}^{CS}, with δ_{iso}^{CS} = -135 ppm · CN + 1405 ppm (R^2 = 0.63) for the non-$LaMO_3$ compounds. Error bars may be obscured by the datum symbol.

Like Willans et al., no relationship was found between the lanthanum coordination number and ^{139}La C_Q (Figure 4).

Chemical Shielding Anisotropy

The quadrupolar interaction is clearly the primary influence on the lineshape of ^{139}La spectra. However, it is clear that CSA can have significant impact, as seen with the spectra of $LaBO_3$, $LaScO_3$, and La_2O_3. Many lanthanum compounds have only been investigated at a single field strength, preventing the collection of accurate CSA parameters. While we have investigated a few samples at two field strengths, the still too small number of data points and their considerable uncertainties render it impossible to draw any conclusions about the relationship between crystal structure and ^{139}La CSA at this time.

Quadrupolar Coupling Constant

The relationships between ^{139}La C_Q values and selected polyhedral distortion parameters are shown in Figure 5. As with the isotropic chemical shift, it is valuable to examine the non-$LaMO_3$ and $LaMO_3$ compounds separately.

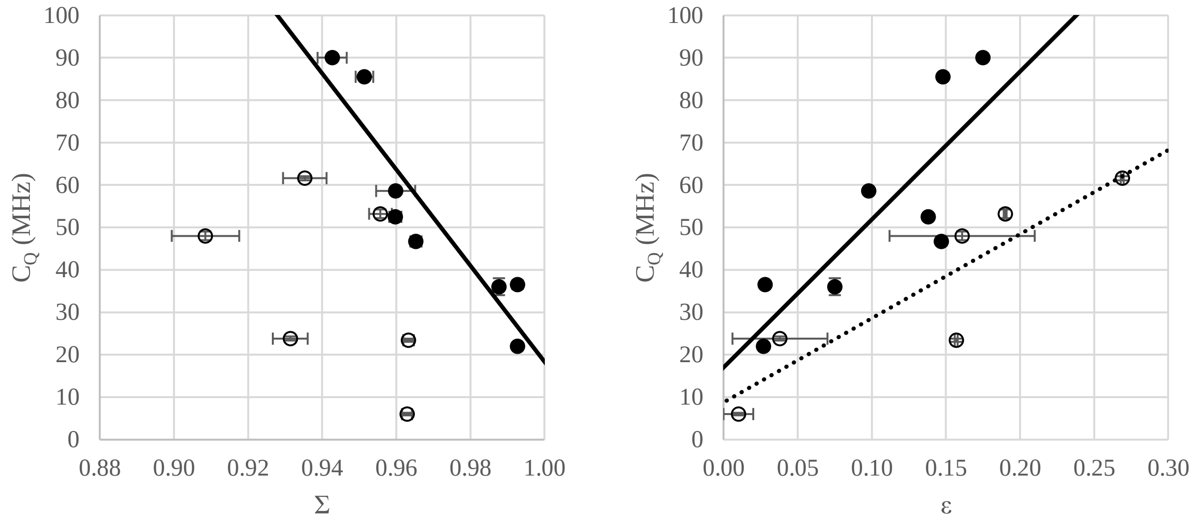

Figure 5. Filled circles (●) indicate compounds of the non-$LaMO_3$ family, while open circles (○) indicate $LaMO_3$ compounds. Left: relationship between ^{139}La C_Q and sphericity (Σ). Right: relationship between ^{139}La C_Q and ellipsoid span (ϵ). The solid lines indicate the relationship between ^{139}La C_Q and the respective distortion parameter of the non-$LaMO_3$ compounds, with: left, C_Q = -1133 MHz · Σ + 1151 MHz (R^2 = 0.85); right, C_Q = 349 MHz · ϵ + 17 MHz (R^2 = 0.68). The dotted line indicates the relationship between ^{139}La C_Q and the ellipsoid span of the $LaMO_3$ compounds, with C_Q = 198 MHz · ϵ + 9 MHz (R^2 = 0.80). Error bars may be obscured by the datum symbol.

Non-$LaMO_3$ Compounds

The non-$LaMO_3$ compounds show a strong negative correlation with the sphericity distortion parameter, with C_Q increasing as sphericity decreases. The uncertainty in the sphericity is relatively low for the non-$LaMO_3$ compounds as compared to the $LaMO_3$ compounds; this is attributed to a wider range of bond lengths present in most $LaMO_3$ compounds.

The quality of the fit of the relationship between the ellipsoid span and C_Q for the non-$LaMO_3$ compounds ($R^2 = 0.68$) is lower than both that of the $LaMO_3$ compounds ($R^2 = 0.79$) and the relationship between Σ and C_Q for the non-$LaMO_3$ compounds ($R^2 = 0.86$). The ellipsoid span is primarily dependent on the shortest and longest semi major ellipsoid axes, e_a and e_c. There is a moderate correlation between C_Q and e_a for the non-$LaMO_3$ compounds (Figure S28b, $R^2 = 0.69$), but not between C_Q and e_c. As such, ϵ is not as good of a descriptor of distortion for the non-$LaMO_3$ compounds, but has the advantage of being generally useful for both non-$LaMO_3$ and $LaMO_3$ compounds.

In an attempt to relate C_Q to specific structural features, the various distortion parameters are plotted against the longest and shortest La-O bonds (d_{max} and d_{min}, respectively). The most relevant plots are presented in Figure 6; the rest can be found in the supporting information. The distortion parameters that best correlate to the C_Q of the non-$LaMO_3$ compounds are generally dependent on d_{max}, suggesting that the C_Q of the non-$LaMO_3$ compounds might be similarly dependent. Unfortunately, this is not the case, as the relationship between C_Q and d_{max} of the non-$LaMO_3$ compounds is less reliable than the relationship between C_Q and either Σ or ϵ (R^2 values of 0.58, 0.85, and 0.68, respectively) for the non-$LaMO_3$ compounds. The quadrupolar coupling constants of the non-$LaMO_3$ compounds seem to be dependent on both d_{min} and d_{max}, and are better fit by a combination of d_{min} and d_{max} than by either alone. The difference between the average La-O bond length (d_{avg}) and the shortest La-O bond length (Figure 7) is the structural parameter which best predicts the ^{139}La C_Q for non-$LaMO_3$ compounds ($R^2 = 0.92$).

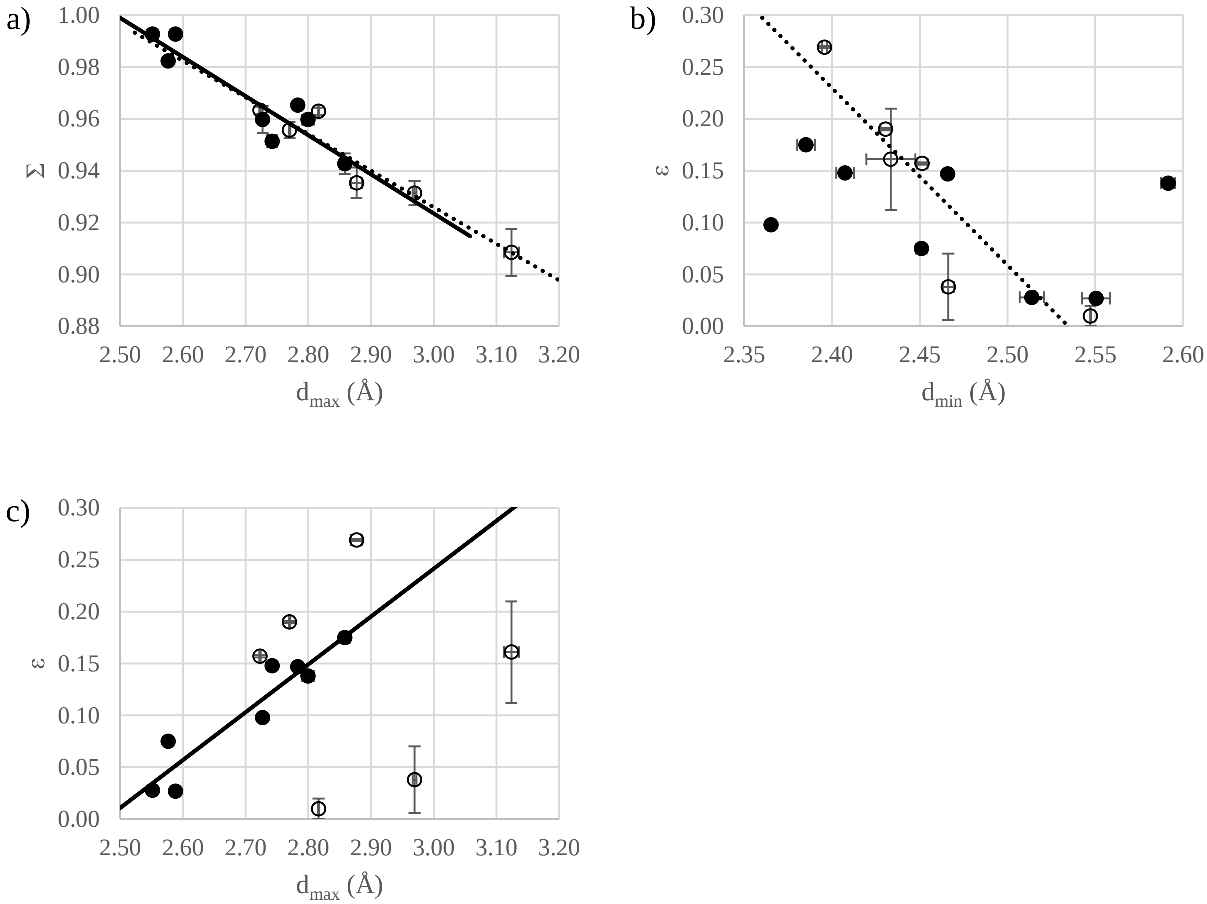

Figure 6. Filled circles (●) indicate compounds of the non-$LaMO_3$ family, while open circles (○) indicate $LaMO_3$ compounds. a) Relationship between sphericity (Σ) and the longest La-O bond length (d_{max}). The solid line indicates the relationship between Σ and d_{max} for the non-$LaMO_3$ compounds, with $\Sigma = -5.71 \frac{1}{\text{Å}} \cdot d_{max} + 8.23$ ($R^2 = 0.86$). The dashed line indicates the relationship between between Σ and d_{max} for the $LaMO_3$ compounds, with $\Sigma = -6.49 \frac{1}{\text{Å}} \cdot d_{max} + 9.00$ ($R^2 = 0.92$). b) Relationship between ellipsoid span (ϵ) and the shortest La-O bond length (d_{min}). The dashed line indicates the relationship between between ϵ and d_{min} for the $LaMO_3$ compounds, with $\epsilon = -0.48 \frac{1}{\text{Å}} \cdot d_{max} + 2.52$ ($R^2 = 0.82$). c) Relationship between ellipsoid span (ϵ) and d_{max}. The solid

line indicates the relationship between between ϵ and d_{max} for the non-$LaMO_3$ compounds, with $\epsilon = 1.92 \frac{1}{Å} \cdot d_{max} + 2.50$ ($R^2 = 0.89$). Error bars may be obscured by the datum symbol.

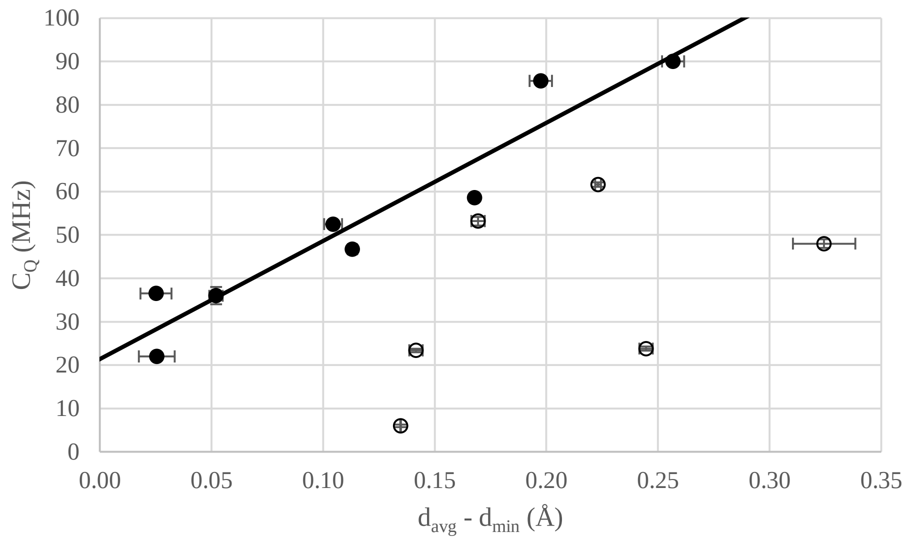

Figure 7. Relationship between the difference of the average La-O bond length (d_{avg}) and the minimum La-O bond length (d_{min}). Filled circles (●) indicate compounds of the non-$LaMO_3$ family, while open circles (○) indicate $LaMO_3$ compounds. The solid line indicates the relationship between the bond length difference and C_Q for the non-$LaMO_3$ compounds, with $C_Q = 272 \frac{\text{MHz}}{Å} \cdot (d_{avg}\text{-}d_{min}) + 21$ MHz ($R^2 = 0.92$). Error bars may be obscured by the datum symbol.

$LaMO_3$ Compounds

In contrast to the strong relationship seen in the non-$LaMO_3$ compounds, the $LaMO_3$ compounds do not show a significant dependence of C_Q on Σ ($R^2 = 0.22$). The compounds that are most likely affecting the relationship between C_Q and Σ for the $LaMO_3$ compounds are $LaCoO_3$

and $LaCrO_3$. As discussed in their respective sections in the supporting information, the $LaCoO_3$ and $LaCrO_3$ coordination polyhedra are cuboctohedra with a large difference between d_{min} and d_{max}; furthermore, the positioning of the longest and shortest La-O bonds in these structures ensures that it is difficult to fit a sphere to the oxygen positions.

The use of the ellipsoid span to relate ^{139}La C_Q and distortion is more effective than the use of Σ for the $LaMO_3$ compounds, though it is difficult to reliably fit an ellipsoid to the lanthanum polyhedra of $LaCrO_3$ and $LaCoO_3$ for the same reasons that it is difficult to fit a sphere; this is reflected in the large uncertainties of ϵ for these compounds. The individual influences of e_a and e_c are examined for the $LaMO_3$ compounds, with e_c having a much stronger relationship with C_Q than e_a. This behaviour is the mirror image of the non-$LaMO_3$ compounds, and indicates the difference between the two families.

Figure 6 highlights additional differences between the $LaMO_3$ and non-$LaMO_3$ compounds. While the sphericity of both families is highly dependent on d_{max}, the ellipsoid span of the $LaMO_3$ compounds is not dependent on d_{max}, but instead on d_{min}. As such, we examine the relationship between C_Q and d_{min} for the $LaMO_3$ compounds (Figure 8). The fit of the relationship between C_Q and d_{min} is comparable in quality to the relationship between C_Q and ϵ (R^2 of 0.84 and 0.80 respectively). The C_Q of the $LaMO_3$ compounds is effectively independent of d_{max}, with an R^2 of 0.06. While the C_Q values of the $LaMO_3$ compounds cannot be explained solely by the shortest La-O bond lengths, they are much more dependent on this parameter than the non-$LaMO_3$ compounds. The differing influences of individual structural parameters also explains why the sphericity poorly relates to $LaMO_3$ C_Q: Σ is strongly dependent on d_{max}, while the C_Q values of $LaMO_3$ compounds are not dependent on d_{max}. We attribute the differences in the behaviour of the $LaMO_3$ and non-$LaMO_3$ compounds with regards to our model parameters primarily due to structural differences between the two compounds. The shortest La-O bonds in the $LaMO_3$ compounds form either ideal or slightly distorted trigonal prisms, whereas this substructure is generally absent from the non-$LaMO_3$ coordination polyhedra. This substructure, when considered in the context of the remaining atoms in the coordination polyhedron, is difficult to fit with either a sphere or an ellipsoid, limiting the generalizability of our models.

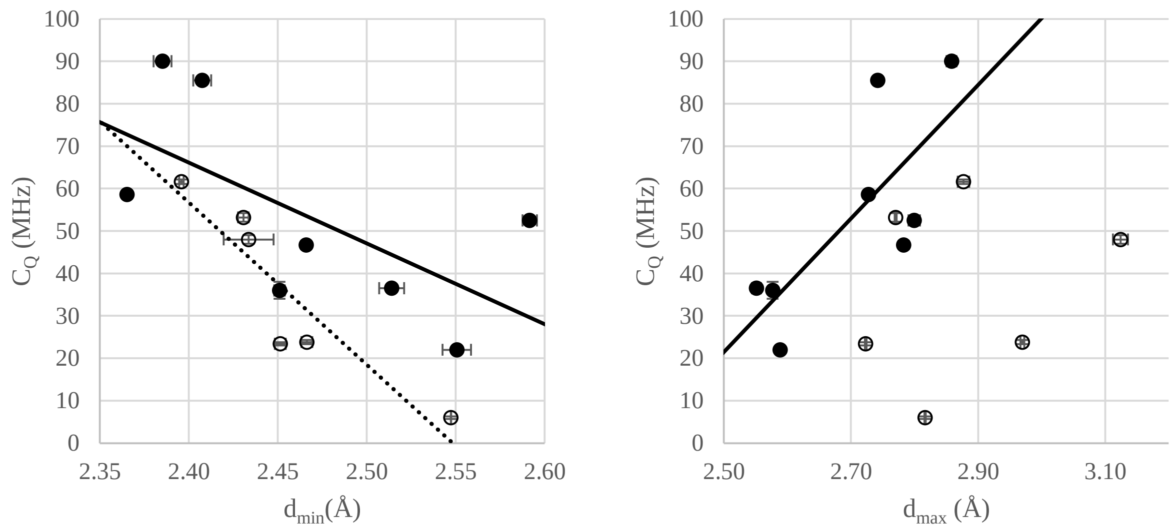

Figure 8. Relationship between minimum and maximum La-O bond lengths and experimental ^{139}La C_Q. Filled circles (●) indicate compounds of the non-$LaMO_3$ family, while open circles (○) indicate $LaMO_3$ compounds. Left: relationship between the shortest La-O bond length (d_{min}) and ^{139}La C_Q. The solid line indicates the relationship between d_{min} of the non-$LaMO_3$ compounds and C_Q, with $C_Q = -191 \frac{MHz}{Å} \cdot d_{min} + 523$ MHz (R^2 = 0.41), while the dotted line indicates the relationship between d_{min} of the $LaMO_3$ compounds and C_Q, with $C_Q = -382 \frac{MHz}{Å} \cdot d_{min} + 974$ (R^2 = 0.84). Right: relationship between the longest La-O bond length (d_{max}) and ^{139}La C_Q. The solid line indicates the relationship between d_{max} of the non-$LaMO_3$ compounds and C_Q, with $C_Q = 157 \frac{MHz}{Å} \cdot d_{max} - 372$ MHz ($R^2 = 0.58$). Error bars may be obscured by the datum symbol.

The most generally applicable distortion parameter is the ellipsoid span, adequately relating the C_Q to distortion for both the $LaMO_3$ and non-$LaMO_3$ compounds. The distortion of the non-$LaMO_3$ compounds is better described by the sphericity parameter. The C_Q values of both $LaMO_3$ and non-$LaMO_3$ compounds can be related to specific structural features. The C_Q of a given $LaMO_3$ compound is related to the length of the shortest La-O bond, while the C_Q of a given non-$LaMO_3$ compound is related to the difference between the average La-O bond length and the shortest La-O bond length.

DFT calculations

The quadrupolar coupling constants calculated with ABINIT generally show good agreement with those determined experimentally (Figure 9), with deviations typically less than either 15% or 3 MHz absolute, depending on the magnitude of C_Q. There are two notable exceptions to this trend: the calculated C_Q values of $LaBSiO_5$ and $LaPO_4 \cdot nH_2O$ are significantly greater than the experimental values, $LaBSiO_5$ by 22% (20.0 MHz) and $LaPO_4 \cdot nH_2O$ by 312% (103.2 MHz).

In both of these cases, the difference between experimental and ab initio results are largely attributed to errors in the experimental structure. An example of the sensitivity of C_Q to crystal structure is $LaBO_3$: calculations carried out on a different $LaBO_3$ structure[46] returned a C_Q of -84 MHz and η of 0.05, with only slight structural differences from the structure used in this study. The error in the calculated C_Q of $LaPO_4 \cdot nH_2O$ has two possible explanations: firstly, the structure used in our calculations does not account for the presence of interstitial water; secondly, as discussed above, there is some debate over the structure of rare earth phosphate hydrates. The C_Q

predicted by the sphericity of the lanthanum site in $LaPO_4 \cdot nH_2O$ is 107.8 MHz, consistent with the ab initio results.

If the two results with the greatest absolute error ($LaPO_4 \cdot nH_2O$ and $LaBSiO_5$) are excluded from the fit, the relationship between experimental and calculated C_Q is very nearly 1:1, with most computational values being slightly overestimated.

The calculations of the asymmetry parameter suffer the same problems as the calculations of the quadrupolar coupling constant: the values of η for $LaPO_4 \cdot nH_2O$ and $LaBSiO_5$ are extremely low as compared to experiment. The large deviation in η is also attributed to errors in the experimental geometry used for the DFT calculations. The values of η for the other systems that were studied are more reliable. Most are constrained to η = 0 by symmetry, which is reflected by the DFT calculations. The few that are not constrained by symmetry generally have calculated values which are reasonably close to experiment.

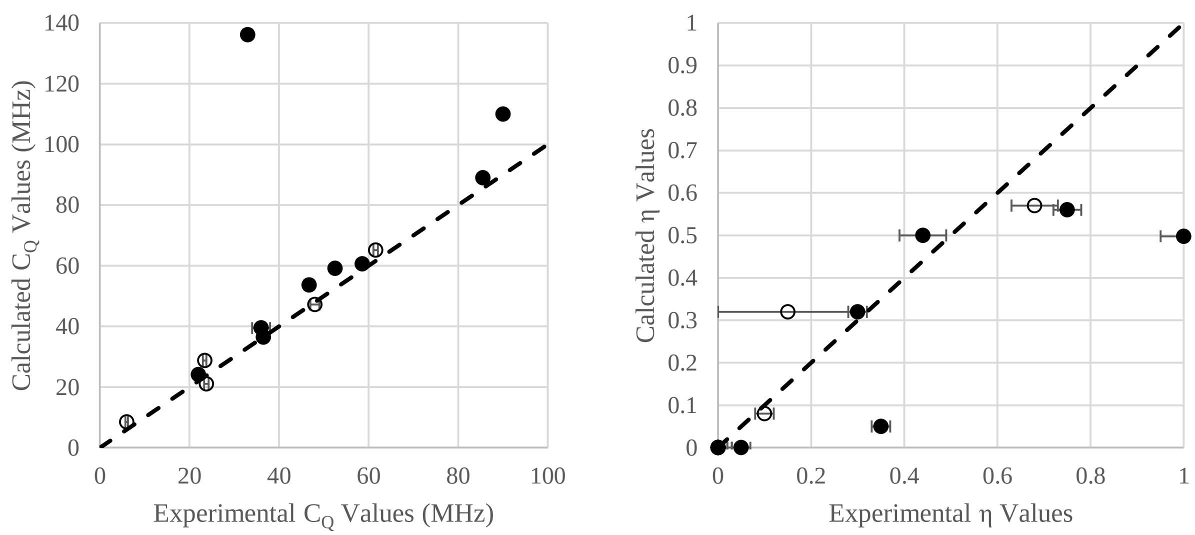

Figure 9. Relationship between experimental and calculated ^{139}La C_Q values (left) and η values (right). Filled circles (●) indicate compounds of the non-$LaMO_3$ family, while open circles (○)

indicate $LaMO_3$ compounds. The dashed line indicates a 1:1 relationship between computational results and experimental results. Error bars may be obscured by the datum symbol.

Differences between $LaMO_3$ and non-$LaMO_3$ compounds

There are no obvious differences between the $LaMO_3$ and non-$LaMO_3$ compounds aside from their general formulae. The coordination numbers of the $LaMO_3$ compounds range from 8 to 12, and examples can be found in the non-$LaMO_3$ compounds which share the same coordination numbers. A mirror plane can be found in the lanthanum polyhedra of most, but not all, $LaMO_3$ compounds, and can also be found in non-$LaMO_3$ compounds. The presence of a threefold rotation axis is not a unifying factor, as some $LaMO_3$ compounds possess this symmetry element, while others do not. Given the complex relationship between the EFG and crystal structure, it is likely that there is no single distinguishing structural feature between the $LaMO_3$ and non-$LaMO_3$ compounds, but instead a combination of features.

Conclusions

In this work we relate two numerical measures of the distortion of coordination polyhedra from spherical symmetry to ^{139}La C_Q. The ^{139}La WCPMG NMR spectra of $LaBO_3$, $LaPO_4 \cdot 1.8H_2O$, $LaBGeO_5$, $LaBSiO_5$, $La_2(SO_4)_3 \cdot 9H_2O$ and $La_2(CO_3)_3 \cdot 8H_2O$ are reported for the first time, and used to supplement existing literature reports of ^{139}La NMR parameters in solid state oxide materials. When examining a broad range of compounds, we find that the behaviour of the

^{139}La C_Q in response to deviations from spherical symmetry divides the examined materials into two families: compounds with the general formula $LaMO_3$, and the rest. The ellipsoid span, ϵ, is effective in relating C_Q to polyhedral distortion for both families of compounds. Non-$LaMO_3$ compounds are better described by the sphericity parameter Σ. Both families of compounds can be related to direct structural features, with the C_Q of $LaMO_3$ compounds being strongly dependent on the shortest La-O bond length and non-$LaMO_3$ compounds exhibiting a more complex relationship. Isotropic chemical shifts of the non-$LaMO_3$ compounds are found to move to lower frequencies with higher coordination number, while there are insufficient data to draw a similar conclusion for the $LaMO_3$ compounds. Ab initio calculations of EFG parameters provide values that generally agree with experiment, with the exceptions of $LaBO_3$, $LaBSiO_5$, and $LaPO_4 \cdot nH_2O$; the failure of ab initio calculations to return values consistent with experiment is attributed to errors in the reported crystal structures.

Acknowledgements

Financial support from the Natural Sciences and Engineering Research Council of Canada (Canada Grant Number RGPIN 261987) is gratefully acknowledged. We appreciate the assistance of Dr. M. Obrovac (TGA and XRD) and Dr. C. Romao (IVTON). This research was enabled in part due to support provided by WestGrid (www.westgrid.ca).

Supporting Information

PXRD and TGA data used for sample verification, specific computational parameters, verbose results and discussion, and additional graphs describing structure-distortion relations. This material is available free of charge via the Internet at http://pubs.acs.org.

References

(1) Tliha, M.; Mathlouthi, H.; Lamloumi, J.; Percheron-Guegan, A. AB_5-Type Hydrogen Storage Alloy Used as Anodic Materials in Ni-MH Batteries. *J. Alloys Compd.* **2007**, *436*, 221–225.

(2) Gupta, P.; Jain, H.; Williams, D. B.; Kanert, O.; Kuechler, R. Structural Evolution of $LaBGeO_5$ Transparent Ferroelectric Nano-Composites. *J. Non. Cryst. Solids* **2004**, *349*, 291–298.

(3) Kehoe, S.; Langman, M.; Werner-Zwanziger, U.; Abraham, R. J.; Boyd, D. Mixture Designs to Assess Composition-Structure-Property Relationships in SiO_2-CaO-ZnO-La_2O_3-TiO_2-MgO-SrO-Na_2O Glasses: Potential Materials for Embolization. *J. Biomater. Appl.* **2013**, *28*, 416–433.

(4) D'Haese, P. C.; Spasovski, G. B.; Sikole, A.; Hutchison, A.; Freemont, T. J.; Sulkova, S.; Swanepoel, C.; Pejanovic, S.; Djukanovic, L.; Balducci, A.; et al. A Multicenter Study on the Effects of Lanthanum Carbonate (Fosrenoltm) and Calcium Carbonate on Renal Bone Disease in Dialysis Patients. *Kidney Int.* **2003**, *63*, 73–78.

(5) Dithmer, L.; Lipton, A. S.; Reitzel, K.; Warner, T. E.; Lundberg, D.; Nielsen, U. G. Characterization of Phosphate Sequestration by a Lanthanum Modified Bentonite Clay: A Solid-State NMR, EXAFS, and PXRD Study. *Environ. Sci. Technol.* **2015**, 150323063204005.

(6) Pyykkö, P. Year-2008 Nuclear Quadrupole Moments. *Molecular Physics*. August 20, 2008, pp 1965–1974.

(7) O'Dell, L. A.; Schurko, R. W. QCPMG Using Adiabatic Pulses for Faster Acquisition of Ultra-Wideline NMR Spectra. *Chem. Phys. Lett.* **2008**, *464*, 97–102.

(8) Thompson, A. R.; Oldfield, E. Solid-State Scandium-45, Yttrium-89, and Lanthanum-139 Nuclear Magnetic Resonance Spectroscopy. *J. Chem. Soc. Chem. Commun.* **1987**, 27.

(9) Dupree, R.; Lewis, M. H.; Smith, M. E. A High-Resolution NMR Study of the Lanthanum-Silicon-Aluminum-Oxygen-Nitrogen System. *J. Am. Chem. Soc.* **1989**, *111*, 5125–5132.

(10) Bastow, T. J. 139La Nuclear Magnetic Resonance Characterisation of La_2O_3 and

$La_{1-x}Sr_xMO_3$ Where M = Cr, Mn or Co. *Solid State Nucl. Magn. Reson.* **1994**, *3*, 17–22.

(11) Hamaed, H.; Lo, A. Y. H.; Lee, D. S.; Evans, W. J.; Schurko, R. W. Solid-State ^{139}La and ^{15}N NMR Spectroscopy of Lanthanum-Containing Metallocenes. *J. Am. Chem. Soc.* **2006**, *128*, 12638–12639.

(12) Ooms, K. J.; Feindel, K. W.; Willans, M. J.; Wasylishen, R. E.; Hanna, J. V; Pike, K. J.; Smith, M. E. Multiple-Magnetic Field ^{139}La NMR and Density Functional Theory Investigation of the Solid Lanthanum(III) Halides. *Solid State Nucl. Magn. Reson.* **2005**, *28*, 125–134.

(13) Willans, M. J.; Feindel, K. W.; Ooms, K. J.; Wasylishen, R. E. An Investigation of Lanthanum Coordination Compounds by Using Solid-State ^{139}La NMR Spectroscopy and Relativistic Density Functional Theory. *Chem. - A Eur. J.* **2006**, *12*, 159–168.

(14) Johnston, K. E.; Mitchell, M. R.; Blanc, F.; Lightfoot, P.; Ashbrook, S. E. Structural Study of $La_{1-x}Y_xScO_3$, Combining Neutron Diffraction, Solid-State NMR, and First-Principles DFT Calculations. *J. Phys. Chem. C* **2013**, *117*, 2252–2265.

(15) Michaelis, V. K.; Kroeker, S. ^{73}Ge Solid-State NMR of Germanium Oxide Materials: Experimental and Theoretical Studies. *J. Phys. Chem. C* **2010**, *114*, 21736–21744.

(16) Spencer, L.; Coomes, E.; Ye, E. Structural Analysis of Lanthanum-Containing Battery Materials Using ^{139}La Solid-State NMR. *Canadian Journal of Chemistry*. 2011, pp 1105–1117.

(17) Herzfeld, J.; Berger, A. E. Sideband Intensities in NMR Spectra of Samples Spinning at the Magic Angle. *J. Chem. Phys.* **1980**, *73*, 6021.

(18) Pan, C.; Lee, Y. J.; Ammundsen, B.; Grey, C. P. ^{6}Li MAS NMR Studies of the Local Structure and Electrochemical Properties of Cr-Doped Lithium Manganese and Lithium Cobalt Oxide Cathode Materials for Lithium-Ion Batteries. *Chem. Mater.* **2002**, *14*, 2289–2299.

(19) Balić Žunić, T.; Makovicky, E. Determination of the Centroid or `the Best Centre' of a Coordination Polyhedron. *Acta Crystallogr. Sect. B Struct. Sci.* **1996**, *52*, 78–81.

(20) Makovicky, E.; Balić-Žunić, T. New Measure of Distortion for Coordination Polyhedra. *Acta Crystallogr. Sect. B Struct. Sci.* **1998**, *54*, 766–773.

(21) Marinkovic, B. A.; Ari, M.; de Avillez, R. R.; Rizzo, F.; Ferreira, F. F.; Miller, K. J.; Johnson, M. B.; White, M. A. Correlation between AO_6 Polyhedral Distortion and Negative Thermal Expansion in Orthorhombic $Y_2Mo_3O_{12}$ and Related Materials. *Chem. Mater.* **2009**, *21*, 2886–2894.

(22) Romao, C. P.; Perras, F. A.; Werner-Zwanziger, U.; Lussier, J. A.; Miller, K. J.; Calahoo, C. M.; Zwanziger, J. W.; Bieringer, M.; Marinkovic, B. A.; Bryce, D. L.; et al. Zero Thermal Expansion in $ZrMgMo_3O_{12}$: NMR Crystallography Reveals Origins of Thermoelastic Properties. *Chem. Mater.* **2015**, *27*, 2633–2646.

(23) Balić Žunić, T.; Vicković, I. IVTON – a Program for the Calculation of Geometrical Aspects of Crystal Structures and Some Crystal Chemical Applications. *J. Appl. Crystallogr.* **1996**, *29*, 305–306.

(24) Kupce, E.; Freeman, R. Adiabatic Pulses for Wideband Inversion and Broadband Decoupling. *J. Magn. Reson. Ser. A* **1995**, *115*, 273–276.

(25) Massiot, D.; Fayon, F.; Capron, M.; King, I.; Le Calvé, S.; Alonso, B.; Durand, J. O.; Bujoli, B.; Gan, Z.; Hoatson, G. Modelling One- and Two-Dimensional Solid-State NMR Spectra. *Magn. Reson. Chem.* **2002**, *40*, 70–76.

(26) Eichele, K.; Wasylishen, R. E. WSolids1. Dalhousie University: Halifax 2009.

(27) Perras, F. A.; Widdifield, C. M.; Bryce, D. L. QUEST—QUadrupolar Exact SofTware: A Fast Graphical Program for the Exact Simulation of NMR and NQR Spectra for Quadrupolar Nuclei. *Solid State Nucl. Magn. Reson.* **2012**, *45-46*, 36–44.

(28) Gonze, X.; Amadon, B.; Anglade, P.-M.; Beuken, J.-M.; Bottin, F.; Boulanger, P.; Bruneval, F.; Caliste, D.; Caracas, R.; Côté, M.; et al. ABINIT: First-Principles Approach to Material and Nanosystem Properties. *Comput. Phys. Commun.* **2009**, *180*, 2582–2615.

(29) Torrent, M.; Jollet, F.; Bottin, F.; Zérah, G.; Gonze, X. Implementation of the Projector Augmented-Wave Method in the ABINIT Code: Application to the Study of Iron under Pressure. *Comput. Mater. Sci.* **2008**, *42*, 337–351.

(30) Marques, M. A. L.; Oliveira, M. J. T.; Burnus, T. Libxc: A Library of Exchange and Correlation Functionals for Density Functional Theory. *Comput. Phys. Commun.* **2012**, *183*, 2272–2281.

(31) Zwanziger, J. W.; Torrent, M. First-Principles Calculation of Electric Field Gradients in Metals, Semiconductors, and Insulators. *Appl. Magn. Reson.* **2008**, *33*, 447–456.

(32) Blöchl, P. Projector Augmented-Wave Method. *Phys. Rev. B* **1994**, *50*.

(33) Jollet, F.; Torrent, M.; Holzwarth, N. Generation of Projector Augmented-Wave Atomic Data: A 71 Element Validated Table in the XML Format. *Comput. Phys. Commun.* **2014**.

(34) Perdew, J.; Burke, K.; Ernzerhof, M. Generalized Gradient Approximation Made Simple. *Phys. Rev. Lett.* **1996**, *77*, 3865–3868.

(35) Belsky, A.; Hellenbrandt, M.; Karen, V. L.; Luksch, P. New Developments in the Inorganic Crystal Structure Database (ICSD): Accessibility in Support of Materials Research and Design. *Acta Crystallogr. Sect. B Struct. Sci.* **2002**, *58*, 364–369.

(36) Furukawa, Y.; Okamura, I.; Kumagai, K.; Goto, T.; Fukase, T.; Taguchi, Y.; Tokura, Y. Electronic Correlations on the Verge of the Mott Transition in $La_{1-x}Sr_xTiO_3$ by $^{47/49}Ti$ and ^{139}La Nuclear Magnetic Resonance. *Phys. Rev. B* **1999**, *59*, 10550–10558.

(37) McAndrew, J.; Scott, T. R. Stillwellite, a New Rare-Earth Mineral from Queensland. *Nature* **1955**, *176*, 509–510.

(38) Sigaev, V. N.; Lotarev, S. V.; Orlova, E. V.; Golubev, N. V.; Koltashev, V. V.; Plotnichenko, V. G.; Komandin, G. A. Structure of Lanthanum-Borogermanate Glass with Stillwellite Composition according to Vibrational Spectroscopy Data. *Glas. Ceram.* **2010**, *67*, 105–108.

(39) Sigaev, V.; Mamonov, A.; Pernice, P.; Aronne, A.; Stefanovich, S. Y.; Bush, A. Pyroelectric Composites Based on $LaBSiO_5$ Stillwellite. *Journal of the European Ceramic Society*. 2000, pp 1225–1229.

(40) Juwhari, H. K.; White, W. B. Luminescence of Rare Earth Borosilicates with the Stillwellite and Related Structures. *Mater. Lett.* **2010**, *64*, 1751–1754.

(41) Kratochvílová-Hrubá, I.; Gregora, I.; Pokorný, J.; Kamba, S.; Zikmund, Z.; Petzelt, J.; Čerňanský, M.; Studnička, V.; Sigaev, V. N.; Smelyanskaya, E. N. Vibrational Spectroscopy of $LaBSiO_5$ Glass and Glass-Crystal Composites. *J. Non. Cryst. Solids* **2001**, *290*, 224–230.

(42) Shaltaf, R.; Juwhari, H. K.; Hamad, B.; Khalifeh, J.; Rignanese, G.-M.; Gonze, X. Structural, Electronic, Vibrational, and Dielectric Properties of $LaBGeO_5$ from First Principles. *J. Appl. Phys.* **2014**, *115*, 074103.

(43) Kaminskii, A. A.; Mill, B. V.; Belokoneva, E. L.; Butashin, A. V. Growth, Structure and Spectroscopy of Lanthanum Borogermanate Crystals $LaBGeO_5$. *Akad. Nauk SSSR, Ser. Neorg. Mater.* **1991**, *27*, 556.

(44) Liferovich, R. P.; Mitchell, R. H. A Structural Study of Ternary Lanthanide Orthoscandate Perovskites. *J. Solid State Chem.* **2004**, *177*, 2188–2197.

(45) J. Mason. *Multinuclear NMR*; Mason, J., Ed.; Springer US: Boston, MA, 1987.

(46) Abdullaev, G. K.; Dzhafarov, G. G.; Mamedov, K. S. Crystal Structure of Lanthanum Orthoborate. *Azerbaidzhanskii Khimicheskii Zhurnal* **1976**, 117–120.

For Table of Contents Only